A State-of-Charge and State-of-Health Joint Estimation Method of Lithium-Ion Battery Based on Temperature-Dependent Extended Kalman Filter and Deep Learning

Shiquan Wang, Kai Ou, Wei Zhang, and Ya-Xiong Wang, *Member, IEEE*

***Abstract*—Accurate estimations of the state of charge (SOC) and state of health (SOH) are crucial for improving battery management techniques. However, batteries are affected by temperature and aging, leading to nonlinear relationships that are more difficult to be characterized. This article proposes an SOC–SOH joint estimation method of lithium-ion battery based on temperature-dependent extended Kalman filter (EKF) and deep learning. First, the battery model state, control, and observation matrices with temperature and capacity variables are created for real-time SOC estimation by using EKF at the local end. Second, battery aging features are extracted and weighted using convolutional neural networks (CNNs) and attention mechanisms and are combined with a gated unit to solve long time series memory problem for SOH estimation at remote computing platform. Finally, the dual time-scale joint model is realized by real-time SOC estimation on the local controller, and the SOH can be calculated on the remote computing platform to correct the available capacity to further update SOC at the end of the discharge. Through 1C discharge rate cycle experimental validation, the root mean square errors of SOC and SOH estimation were within 1%. Therefore, the proposed joint SOC–SOH estimation method can be achieved with local and remote computation.**

***Index Terms*—Hybrid neural networks, joint estimation, lithium-ion battery, local and remote computing platforms, state of charge (SOC), state of health (SOH).**

I. Introduction

THE development of lithium-ion battery technology has increased the performance of electric vehicle application and integration of renewable energy with grid. Many studies have focused on battery safety and performance [1]. The battery management system (BMS) collects lithium-ion battery operating data, monitors status, and prevents over charge and over discharge, thereby improving utilization performance [2]. The BMS provides security and balanced management by monitoring and estimating state of charge (SOC) and state of health (SOH) [3]. The accuracy of SOC and SOH estimation can provide strong data support for BMS decision and system performance [4], [5], [6].

SOC cannot be directly measured by experimental means [7]. The current integration, the open circuit voltage (OCV) method, the model-based, and the data-based methods are the most commonly used to determine the SOC [8]. The original battery SOC value determines the accuracy of the current integration method [9]; OCV needs to be measured after the battery has been sitting for more than an hour, making it difficult to update the SOC in time [10]; the data-based estimation methods need to collect a large amount of experimental data from the battery in advance for training, which requires high computational power of the hardware [11]. The battery equivalent circuit model (ECM) method has been extensively studied in the literature. Combined with extended Kalman filter (EKF), unscented Kalman filter (UKF), particle filter (PF), and other improved filtering methods, the battery state equation could be developed by using ECM for SOC estimation [12], [13], [14]. However, the existing SOC estimation models usually describe the basic dynamic characteristics and ignore the effects of self-discharge, aging, and the internal temperature of the battery. Shu et al. [15] proposed an improved recursive least square method for identification and used H-infinity filter for battery SOC estimation; the maximum absolute error (MAE) was less than 1.2% through verification under different temperatures and aging. Tang et al. [16] proposed the temperature-compensated battery model, and then the base model was migrated by using PF to accommodate the internal temperature uncertainties; the SOC estimation error remained at 1.64% when the temperature changed up to 40°C.

SOH is primarily characterized by capacity or internal resistance [17], [18], [19]. Many researchers have developed deep learning methods for SOH estimation. This method does not require a model of the internal mechanism and electrochemical process of the battery but trains the nonlinear mapping relationship between the features and SOH in the charge and discharge

Manuscript received 10 January 2024; revised 14 April 2024 and 12 May 2024; accepted 22 May 2024. Date of publication 4 July 2024; date of current version 12 November 2024. This work was supported in part by Science and Technology Major Project of Fujian Province of China under Grant 2022HZ028018 and in part by the National Natural Science Foundation of China under Grant 51907030. *(Corresponding author: Ya-Xiong Wang.)*

Shiquan Wang, Kai Ou, and Ya-Xiong Wang are with the School of Mechanical Engineering and Automation, Fuzhou University, Fuzhou 350108, China (e-mail: 220227031@fzu.edu.cn; oukai@fzu.edu.cn; yxwang@fzu.edu.cn).

Wei Zhang is with Geo Micro Devices (Xiamen) Company Ltd., Xiamen 361026, China (e-mail: wei.zhang@gmdsemi.com).

Digital Object Identifier 10.1109/TIE.2024.3409912

process formulated by neural networks [20]. Fan et al. [21] used convolutional neural network (CNN)–gate recurrent unit (GRU) for SOH estimation, and the current, voltage, and temperature during battery charging were employed as input; the proposed method was verified on the National Aeronautics and Space Administration (NASA) and Oxford datasets, and the errors of estimation were controlled within 4.3%. Zhang et al. [22] used extended residual regression network estimation for SOH estimation, and the incremental capacity and voltage were taken as the characteristic matrix and verified by different charging and incomplete charging modes. However, the battery aging experiment period is long, and the SOH estimation studied in most literatures is based on the public battery dataset. Aging experiments on battery samples are rarely used to validate SOH estimation in practice.

There is a coupling relationship between SOC and SOH. Changes in SOH affect the accuracy of SOC estimation, and changes in SOC also determine the aging speed of the battery [23]. Therefore, the joint estimation of SOC and SOH has received more attention from researchers. Some researchers have used model-based methods in both SOC and SOH estimation. Jiang et al. [24] used adaptive EKF for SOC estimation, recursive total least squares for battery capacity calculation, and finally created a cumulative threshold to achieve the variable multi time-scale joint estimation; the maximum error of SOC estimation under the urban dynamometer driving schedule condition was 3.3%. However, the model-based approach depends on the accuracy of the model. Because of the coupling between SOC and SOH, when the modeling is inaccurate, the joint estimation error of the battery state will be exacerbated. Some researchers also used data-based methods to achieve joint estimation of SOC and SOH. Li et al. [25] used CNN to joint estimation of SOC and SOH through current, voltage, temperature, and other parameters collected by fiber optic sensors; under 1C discharge rate aging experiment, SOC estimation standard deviation decreased by 42.7%. While the data-based approach for joint battery state estimation offers higher accuracy, it requires time-consuming and computationally intensive training data, posing significant challenges for real-time SOC estimation in practical applications. In addition, some researchers had proposed joint estimation based on data-based approach and model. Song et al. [26] introduced the battery performance degradation index extracted through measurable current and voltage and used machine learning and PF for battery states joint estimation.

However, there are still the following problems needed to be addressed:

1) The coupling relationship between temperature, SOC, and SOH is not explained in detail, and the changes in tracking battery model parameters cannot be accurately matched in the joint estimation of SOC–SOH, resulting in reduced calculation accuracy.
2) The degree of correlation between aging characteristics and SOH is inconsistent, and time steps and input feature weighting are not taken into consideration.

To solve the abovementioned problems, the SOC–SOH joint estimation for lithium-ion batteries based on temperature-dependent EKF and deep learning is proposed. In comparison to previous studies on SOC–SOH joint estimation, this article makes the following contributions: 1) The battery model state control and observation equation containing temperature and capacity variables are built in the developed EKF for SOC estimation in real-time on local end controller, and the internal resistance, polarization parameters and OCV at unsampled temperature points are obtained by Lagrange interpolation. 2) The SOH deep learning model is developed on remote computing platform, where CNN is used to capture SOH-related battery aging characteristics, and GRU is used to extract the correlation between time series data and SOH. Meanwhile, attention mechanism (AM) is introduced to weight important temporal features to strengthen the correlation with SOH. 3) An SOC–SOH dual time-scale joint estimation method is proposed. The SOC is estimated in real-time at local controller and the SOH is calculated on a remote computing platform after discharge, and the result is used to correct the battery maximum available capacity for further update SOC.

The remainder of this article is organized as follows: Section II introduces temperature-dependent battery SOC estimation. Section III displays SOH estimation based on deep learning model. Section IV exhibits the result of the SOC-SOH joint estimation. The last part is the conclusion of this article.

II. Temperature-Dependent Battery SOC Estimation

A. Battery ECM Considering the Effect of Temperature

The temperature-dependent Thevenin battery model is shown in Fig. 1, where, I is current; U_t is model output voltage; U_{ocv} is OCV; R_0 is Ohmic internal; R_p is polarization internal resistance; C_p is capacitance of polarization; U_p is the corresponding polarization voltage [27].

The y includes R_0, R_p, C_p, and U_{ocv} and is defined as functional equations related to the temperature T, at time k

$$y_k = f_y(\text{SOC}_k, T_k). \tag{1}$$

According to Kirchhoff definition, the Thevenin battery model is represented by using (2) and (3)

$$U_{t,k} = f_{U_{\text{ocv}}}(\text{SOC}_k, T_k) - I_k f_{R_0}(\text{SOC}_k, T_k) - U_{p,k} \tag{2}$$

$$U'_{p,k} = \frac{I_k}{f_{C_p}(\text{SOC}_k, T_k)} - \frac{U_{p,k}}{f_{C_p}(\text{SOC}_k, T_k) f_{R_p}(\text{SOC}_k, T_k)}. \tag{3}$$

The link of OCV–SOC–T in the discharge process is built by measuring the OCV under charge and discharge circumstances [28].

In the hybrid power pulse characteristic (HPPC) test, the voltage change at the instant of battery pulse charging and discharging can be used to identify R_0. At the initial discharge stage, the voltage drops exponentially, which corresponds to zero-state response of the system state. The voltage profile is fitted for identification R_p (SOC_k,T_k) by a customized function.

$$U_{t,k} = U_{\text{ocv}}(\text{SOC}_k, T_k) - I_k R_0(\text{SOC}_k, T_k) - I_k R_p(\text{SOC}_k, T_k)(1 - e^{-t/\tau}) \tag{4}$$

where, τ is the time constant, $\tau = R_p$ (SOC_k,T_k) $\times$ C_p (SOC_k,T_k).

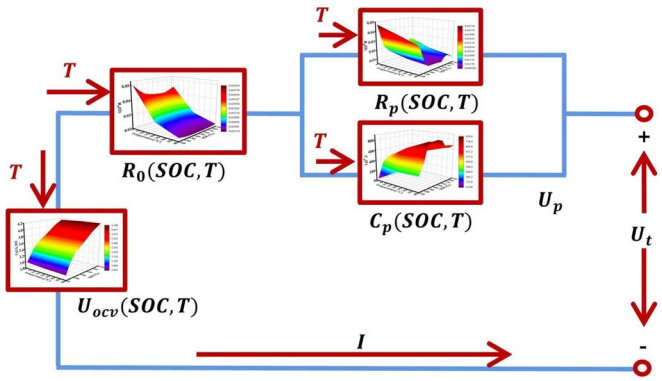

Fig. 1. Thevenin battery model.

When the end of the discharge is standing, this corresponds to zero-input response of the system state. The voltage profile is fitted for identification C_p (SOC_k,T_k) by a custom function.

$$U_{t,k} = U_{\mathrm{ocv}}(\mathrm{SOC}_k, T_k) - I_k R_0(\mathrm{SOC}_k, T_k) - e^{-t/\tau} U_{p,k}. \quad (5)$$

The result of parameters identification is shown in Fig. 2. In the full SOC range, R_0 decreased with the increase of temperature, while C_p showed the opposite trend, and the change was more significant in low temperature environment. In the middle SOC range (30–70%), R_p had no significant change with temperature, but in general, R_p gradually decreased with the increase of temperature. U_{ocv} showed an overall decreasing trend under high temperature environment. Based on the above analysis, R_0, R_p, C_p, and U_{ocv} at different temperatures need to be determined next.

B. Lagrange Interpolation

There is a relationship between battery model parameters and temperatures, $y = f(T)$, $T \in [0\,^\circ\mathrm{C}, 40\,^\circ\mathrm{C}]$. There exists an interpolation function $L(T)$ for the value $y_0, \ldots, y_n$ on $0\,^\circ\mathrm{C} \le T_0 < \ldots < T_n \le 40\,^\circ\mathrm{C}$. The polynomial obtained by applying the Lagrange interpolation formula is shown as follows:

$$L_n(T) = \sum_{k=0}^{n} y_k l_k(T) \quad (6)$$

where $l_x(T)$ is the interpolation basis function

$$l_k(T) = \frac{(T - T_2)(T_1 - T_3)(T - T_n)}{(T_1 - T_2)(T_1 - T_3)(T_1 - T_n)}. \quad (7)$$

According to the identification results at 0 °C, 20 °C and 40 °C, the Lagrange interpolation function $L_n(T)$ can be constructed to calculate R_0, R_p, C_p, and U_{ocv} of temperature sampling points in the range of 0–40 °C. The R_0, R_p, C_p, and U_{ocv} of the battery at 10 °C and 25 °C are shown in Table I.

C. SOC Estimation Based on EKF

The SOC is defined by integrating the current over time, and the discrete form is given by (8) [29]

$$\mathrm{SOC}_{k+1} = \mathrm{SOC}_k + \frac{-\eta I_k t}{Q_{\max}} \quad (8)$$

where SOC_k is SOC at time k; η stands for the coulomb efficiency; $Q_{\max}$ describes current maximum capacity.

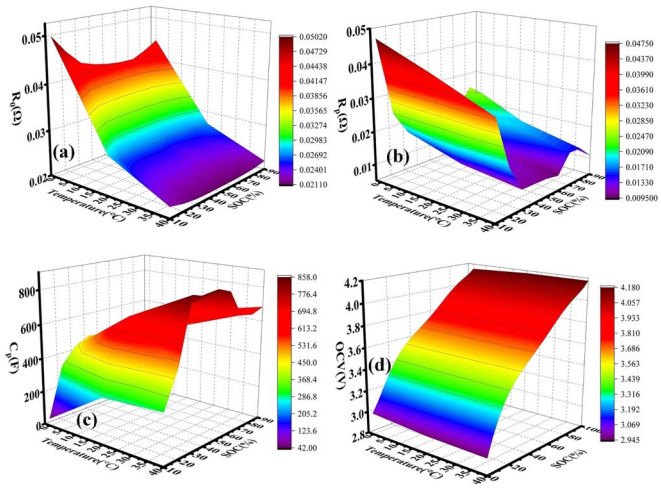

Fig. 2. Results of parameter identification at different temperatures: (a) for R_0; (b) for R_p; (c) for C_p; (d) for U_{ocv}.

The state variables of the battery system is defined as $x_k = [\mathrm{SOC}_k\ U_{p,k}]^T$. The state matrix, control matrix, and observation matrix of the battery system are as follow:

$$\begin{cases} A_k = \begin{bmatrix} 1 & 0 \\ 0 & e^{-t/\tau} \end{bmatrix} \quad C_k = \begin{bmatrix} \dfrac{\partial f_{U_{\mathrm{ocv}}}(\mathrm{SOC}_k, T_k)}{\partial \mathrm{SOC}_k} & -1 \end{bmatrix} \\ B_k = \begin{bmatrix} \dfrac{-\eta t}{Q_{\max}} \\ f_{R_p}(\mathrm{SOC}_k, T_k)(1 - e^{-t/\tau}) \end{bmatrix} \end{cases}. \quad (9)$$

Measured current I_k, measured voltage y_k, and temperature T_k serve as the input of EKF method, and output is the x_k.

The EKF is performed by predicting the system state at each time step, and then corrected by the measurement state. The specific implementation process of SOC estimation based on EKF is as follows [30].

Step 1: Initialization parameters:

The system state is defined as $x_0 = [\mathrm{SOC}_0,\ U_{p,0}]$; the error covariance matrix is calculated by $P_0 = E[(x_0\text{-}x_0^+)(x_0\text{-}x_0^+)^{\mathrm{T}}]$; the noise covariance are represented by R, Q.

The time step cycle is defined as $k = 1, 2, \ldots, N$:

Step 2: Forecasting:

Step 2-1: The current state is estimated based on the optimal state of the previous time:

$$\hat{x}_{\bar{k}+1} = \begin{bmatrix} 1 & 0 \\ 0 & e^{-t/f_{R_p}(\mathrm{SOC}_k, T_k)} \end{bmatrix} \hat{x}_k + \begin{bmatrix} \dfrac{-\eta t}{Q_{\max}} \\ f_{R_p}(\mathrm{SOC}_k, T_k)(1 - e^{-t/\tau}) \end{bmatrix} I_k. \quad (10)$$

Step 2-2: The prior estimation error covariance matrix:

$$P_{\bar{k}+1} = \begin{bmatrix} 1 & 0 \\ 0 & e^{-t/\tau} \end{bmatrix} P_k \begin{bmatrix} 1 & 0 \\ 0 & e^{-t/\tau} \end{bmatrix}^T + Q. \quad (11)$$

Step 3: Measurement and calibration:

TABLE I
BATTERY MODEL PARAMETERS AT 10 °C AND 25 °C

Temperature	Model parameters	SOC 90%	SOC 80%	SOC 70%	SOC 60%	SOC 50%	SOC 40%	SOC 30%	SOC 20%	SOC 10%
10 °C	R_0 (Ω)	0.0337	0.0325	0.0314	0.0310	0.0315	0.0316	0.0313	0.0333	0.0353
	Rp (Ω)	0.0187	0.0221	0.0191	0.0156	0.0162	0.0157	0.0143	0.0230	0.0334
	C_p (F)	483.52	451.38	486.06	549.72	516.24	589.17	631.75	455.15	247.58
	Uocv (V)	4.09	4.02	3.93	3.83	3.73	3.65	3.55	3.43	3.23
25 °C	R_0 (Ω)	0.0256	0.0245	0.0240	0.0238	0.0240	0.0241	0.0243	0.0247	0.0265
	Rp (Ω)	0.0139	0.0179	0.0180	0.0114	0.0121	0.0126	0.0123	0.0200	0.0377
	Cp (F)	612.98	595.07	573.63	665.30	764.18	716.12	783.47	570.81	281.43
	U_{ocv} (V)	4.09	4.02	3.94	3.84	3.74	3.65	3.56	3.43	3.24

Step 3-1: Calculate the prior estimation error:

$$\varepsilon_k = y_k - [f_{U_{\text{ocv}}}(\text{SOC}_k, T_k) - I_k f_{R_0}(\text{SOC}_k, T_k) - U_{p,k}]. \tag{12}$$

Step 3-2: Calculate the Kalman gain:

$$K_k = \frac{P_{\bar{k}+1}\left[\frac{\partial f_{U_{\text{ocv}}}(\text{SOC}_k, T_k)}{\partial \text{SOC}_k} - 1\right]^T}{\left[\frac{\partial f_{U_{\text{ocv}}}(\text{SOC}_k, T_k)}{\partial \text{SOC}_k} - 1\right] P_{\bar{k}+1}\left[\frac{\partial f_{U_{\text{ocv}}}(\text{SOC}_k, T_k)}{\partial \text{SOC}_k} - 1\right]^T + R}. \tag{13}$$

Step 3-3: Update the system state:

$$\hat{x}_{k+1} = \hat{x}_{\bar{k}+1} + K_k \varepsilon_k. \tag{14}$$

Step3-4: Update the error covariance:

$$P_{k+1} = \left(E - K_k\left[\frac{\partial f_{U_{\text{ocv}}}(\text{SOC}_k, T_k)}{\partial \text{SOC}_k} - 1\right]\right) P_{\bar{k}+1}. \tag{15}$$

The new European driving cycle (NEDC) condition was applied to the battery sample (SONYUS18650VTC6) under 10 °C and 25 °C, respectively. The nominal capacity of the battery was 3000 mAh, and the nominal voltage was 3.6 V, and the charge and discharge cut-off voltage were 4.2 V and 2.5 V, respectively. The voltage estimation results are shown in Fig. 3. Under the dynamic conditions of NEDC, the model output voltage could effectively track the measured voltage. When the battery was fully charged, the voltage estimation error was less than 60 mV, and the error was larger near the end of discharge. The voltage estimation error results are shown in Table II. The MAEs and root mean square errors (RMSEs) of voltage estimation at 10 °C and 25 °C remained within 20 mV. Therefore, the presented battery model had a high accuracy.

To verify the performance of the proposed SOC estimation method by taking into account the temperature effect, the fixed battery model parameters were used for comparison, and the results are shown in Fig. 4. The proposed temperature-dependent EKF could rapidly converge to the reference within 500 s with an initial SOC error of 6%, and then the SOC estimation error was kept within 1.5%. The accuracy and robustness of SOC estimation, considering the temperature influence, were superior to those without. The MAEs and RMSEs of SOC estimation at 10 °C and 25 °C were less than 1.2%. The results showed that matching the pairs of battery model parameters R_0, R_p, C_p, and U_{ocv} in the EKF method corresponding to the experimental environment could improve the accuracy of SOC estimation.

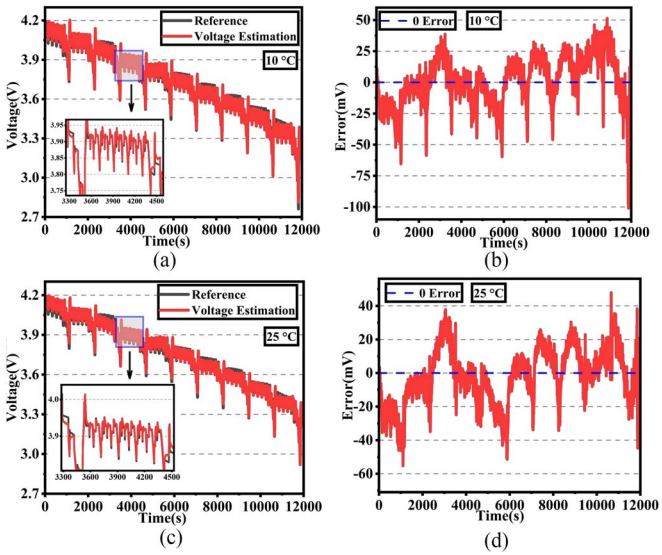

Fig. 3. Results of model output voltage estimation. (a) Model output voltage estimation at 10 °C. (b) Error of model output voltage estimation at 10 °C. (c) Model output voltage estimation at 25 °C. (d) Error of model output voltage estimation at 25 °C.

III. SOH ESTIMATION BASED ON DEEP LEARNING MODEL

A. SOH Definition and Data Preprocessing

SOH is defined as the change in the battery's available capacity [31], where Q_n is the nominal capacity.

$$\text{SOH} = \frac{Q_{\max}}{Q_n}. \tag{16}$$

Five kinds of measurable data: cycle number Nc, discharge current I, discharge voltage V, temperature T, and discharge time Ti, are defined as the deep learning model input, $X_k = [Nc_k, I_k, V_k, T_k, Ti_k]$, and SOH is the output, $Y_k = [\text{SOH}_k]$. To enhance the stability of the model, the X_k needs to be normalized.

$$X_k' = \frac{X_k - \min\ (X_k)}{\max\ (X_k) - \min\ (X_k)} \tag{17}$$

where X_k' is normalized data; $\min(X_k)$ is minimum value in X_k; $\max(X_k)$ is maximum value in X_k.

TABLE II
MAE AND RMSE OF EKF MODEL UNDER DIFFERENT TEMPERATURES

Model	Criteria	10 °C	25 °C
Voltage estimation	MAE (mV)	15.32	13.54
	RMSE (mV)	19.16	16.92
Temperature consideration	MAE (%)	0.84	0.68
	RMSE (%)	0.94	0.73
With initial error	MAE (%)	1.09	0.89
	RMSE (%)	1.12	0.94
Temperature not consideration	MAE (%)	1.63	2.13
	RMSE (%)	2.16	2.35

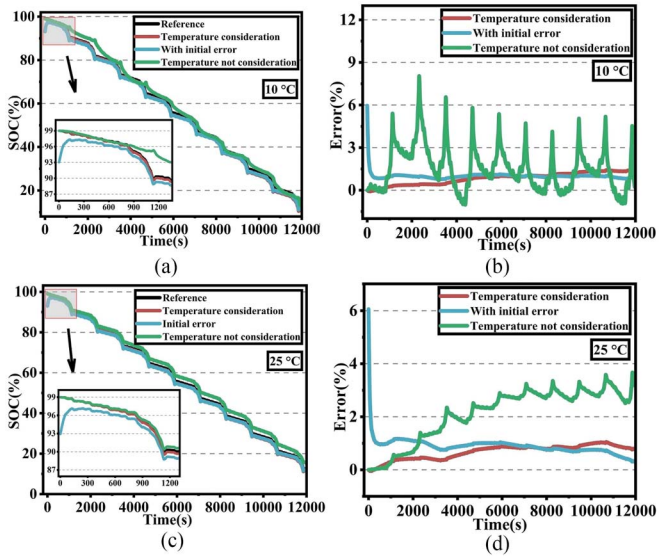

Fig. 4. Results of SOC estimation. (a) SOC estimation at 10 °C. (b) Error of SOC estimation at 10 °C. (c) SOC estimation at 25 °C. (d) Error of SOC estimation at 25 °C.

B. CNN–GRU–AM Model

CNN has certain advantages in feature extraction, and GRU is suitable for dealing with time series problems [32]. Therefore, by combining CNN and GRU, the AM is used to weight various factors of the input, reduce the weight of factors with low correlation with the real SOH, and pay more attention to factors with high correlation. The schematic diagram of SOH estimation is presented in Fig. 5(a).

In the CNN layer, the input data X_k' are first convolved by customizing the convolution kernel size to generate the characteristic data related to Nc, I, V, T, and Ti. The maximum pooling layer is introduced into the CNN layer to decrease the dimensionality of the data. The input data are all of the time series type. Therefore, one-dimensional forms are used in convolution and pooling operations.

$$X_k{}^l = f\left(\sum_{i=1}^{J} X_i' * w_c + b_c\right) \tag{18}$$

$$X_k^l = \text{Maxpool}(X_k^l) \tag{19}$$

where $f(\cdot)$ is the activation function; J is convolution mapping number; * is convolution process; Maxpool$(\cdot)$ is the maximum pooling function, which select the maximum value in each area as output; w_c and b_c are convolution kernel weights and bias, respectively.

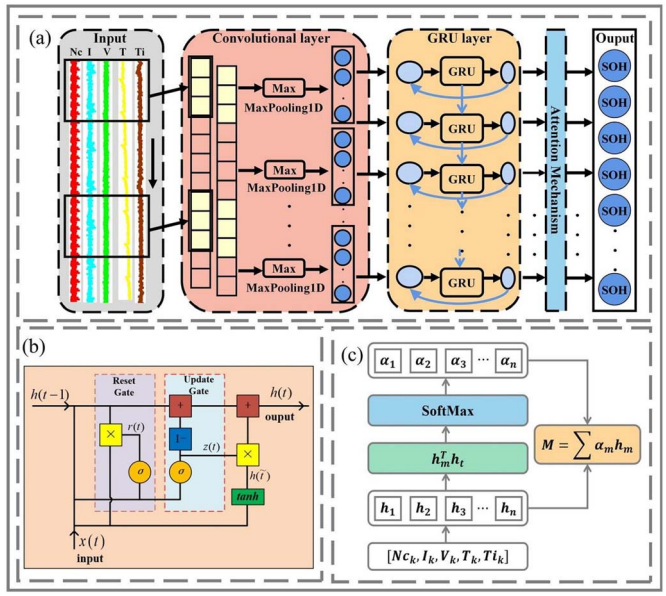

Fig. 5. Schematic diagram of CNN-GRU-AM deep learning model. (a) Overall scheme. (b) Internal structure of GRU unit. (c) AM calculation process.

However, the battery discharge data have strong time dependence and the length of data series is large. In the GRU model, there is a reset gate, which determines how to combine previous data with current input, and an update gate, determining the amount of original data to be saved. The GRU structure is shown in Fig. 5(b).

$$z_k = \sigma(w_z[H_{k-1}, X_k^l] + b_z) \tag{20}$$

$$r_k = \sigma(w_r[H_{k-1}, X_k^l] + b_r) \tag{21}$$

where z is the update gate; r is the reset gate; h is the hidden state; σ is the activation, which converts the data to the range [0,1]; w_z and w_r are weight values; b_z and b_r are parameters of the bias.

The output of the GRU unit is hidden state $H_k = [h_{1,k}, h_{2,k}, \ldots, h_{n,k}]$; $H_{\tilde{k}}$ is temporary hidden state; n is number of hidden units.

$$H_{\tilde{k}} = \tanh(w_g[r_k \cdot H_{k-1}, X_k^l] + b_g) \tag{22}$$

$$H_k = (1 - z_k) \cdot H_{k-1} + z_k \cdot H_{\tilde{k}} \tag{23}$$

where tanh is activation function, which converts the data to the range [−1,1]; w_g is weight value; b_g is parameter of the bias.

The correlations between SOH and each input battery aging characteristic are different. By introducing AM, the different input battery aging characteristics can be formulated.

The hidden state H of the GRU output is weighted by the AM to get new output vector M, as shown in Fig. 5(c). The importance weight α_t of h_t is calculated as shown in (24)

$$\alpha_m = \frac{e^{s(h_m,h_t)}}{\sum_{m=1}^{n} e^{s(h_m,h_t)}} \tag{24}$$

where h_m is the hidden status at the current time; h_t represents the state associated with the current task in the input state vector; s is attention scoring function of the m hidden unit, as shown in (25)

$$s(h_m, h_t) = h_m^T h_t. \tag{25}$$

Finally, the input features are summarized by weighted average to obtain a new output vector M, as shown in (26)

$$M = \sum_{\mathrm{m}=1}^{n} \alpha_m h_m. \tag{26}$$

Based on AM, the SOH is estimated by weighted battery aging characteristics. The output results after the fully connected layer are as follows:

$$\mathrm{SOH}_k = \sigma(w_0 M + b_0) \tag{27}$$

where SOH_k is the output of the AM model at time step k; w_0 and b_0 represent the weight and bias of the fully connected layer, respectively.

The MAE loss function is defined as the difference between the SOH estimation value and reference.

$$\mathrm{MAE} = \frac{1}{k}\sum_{i=1}^{k} |\mathrm{SOH}_k - \mathrm{SOH}_k'| \tag{28}$$

where SOH_k' is the real SOH. To minimize the loss function, the weight parameters (w_c, w_z, w_r, w_g, w_0) and bias parameters (b_c, b_z, b_r, b_g, b_0) in the CNN–GRU–AM model are dynamically updated by Adam optimization algorithm, so that the SOH estimation is close to the real value. The pseudocode of the CNN–GRU–AM-based SOH estimation is summarized in Table III.

The samples B0005 and B0006 and B0007 from the NASA dataset and lithium-ion batteries for NEDC testing were taken as experimental objects [33]. The initial capacities of samples were 1.86 Ah, 2.04 Ah, 1.89 Ah, and 2.85 Ah, respectively. The batteries were charged in the constant current constant voltage (CC–CV) method, then were discharged in the constant current (2 A) to 2.7 V, 2.5 V, and 2.2 V, respectively. The battery in the laboratory test was cyclically discharged to 2.5 V under the NEDC condition. The experiment was stopped when the batteries capacity dropped to 1.32 Ah, 1.19 Ah, 1.43 Ah, and 2.74 Ah, respectively.

The first 70% of the discharge process data from the NASA datasets and experimental datasets were used for training, and the last 30% of the discharge process data were used for SOH estimation. When the network parameters of the same model were set uniformly, the SOH estimation accuracy of GRU is better than that of LSTM. Compared with GRU and CNN–GRU, introducing AM into the model could assign higher computational weights to strongly correlated features. Moreover, to verify the generalization ability of the proposed method, the battery 80% depth of discharge (DOD) data, SOC from 90% to 10%, were used as input for SOH estimation, and the results are shown in Fig. 6 and Table IV. The maximum difference between two DOD conditions of MAE and RMSE of the SOH estimation was 0.05% and 0.08%, respectively.

TABLE III
SOH ESTIMATION PSEUDOCODE BASED ON CNN–GRU–AM

Algorithm: SOH estimation based on CNN–GRU–AM

Input: *X=[Nc, I, V, T, Ti], filters F, kernel_size Ks, activation_cnn Ac, strides S, input_shape Is, pool_size Ps, gru_cell Gc, activation_gru Cg, attention_cell Atc, dense_cell dc, activation_dense Ad, learning_rate η*
Output: *Y=[SOH]*
Divide *X* into X_{train}, X_{test} and *Y* into Y_{train}, Y_{test}
Preprocessing: $Norm_{min\text{-}max}(Xtrain) \rightarrow Xtrain'$
Design CNN_{net} by *F, Ks, Ac, S, Is*, Ps, and GRU_{net} by *Gc, Cg*, and $\mathrm{Attention}_{net}$ by *Atc*, and Dense_{net} by *dc, Ad*
Initialize the input of CNN_{net}, GRU_{net}, $\mathrm{Attention}_{net}$, and Dense_{net}
For each step ∈ [1, steps_{train}] **do**
    $\mathrm{CNN}_{net}(X_{train}') \rightarrow X_{train}^{l}$
    $\mathrm{GRU}_{net}(X_{train}^{l}) \rightarrow H_{train}$
    $\mathrm{Attention}_{net}(H_{train}) \rightarrow M_{train}$
    $\mathrm{Dense}_{net}(M_{train}) \rightarrow Y_{train}'$
    $1/k\sum_{i=1}^{k} |Y_{train} - Y_{train}'| \rightarrow \mathrm{loss}$
    Update CNN_{net}, GRU_{net}, $\mathrm{Attention}_{net}$, Dense_{net} by *loss* and *η*
End for
Get and **save** $\mathrm{CNN\text{-}GRU\text{-}AM}_{net}$ as $\mathrm{CNN\text{-}GRU\text{-}AM}_{net}$*
Preprocessing: $Norm_{min\text{-}max}(X_{test}) \rightarrow X_{test}'$
For each step ∈ [1, steps_{test}] **do**
    $\mathrm{CNN\text{-}GRU\text{-}AM}_{net}^{*}(X_{test}') \rightarrow Y_{test}'$
End for

IV. JOINT SOC–SOH ESTIMATION

A. Dual Time-Scale Joint Estimation

As the SOH changes during actual battery use, the accuracy of monitoring the SOC decreases. Therefore, timely updating of variables reflecting battery aging should be required in the SOC estimation model.

In the proposed EKF for SOC estimation, the capacity characteristics of the reaction SOH are set as variables to obtain a new control matrix B_k, as shown in (29). The SOH conversion process is $Q_{\max} = Q_n \times \mathrm{SOH}$.

$$B_k = \begin{bmatrix} \dfrac{-\eta t}{Q_{\max}(\mathrm{SOH})} \\ f_{R_p}(\mathrm{SOC}_k, T_k)(1 - e^{-t/\tau}) \end{bmatrix}. \tag{29}$$

Fast update frequency is required by SOC for system status monitoring. However, the frequency of SOH changes is slow, and its impact on the charge/discharge process can be neglected. Based on SOC and SOH variation characteristics, a dual time-scale joint estimation is proposed. During the discharging process, EKF is used for real-time SOC estimation, while SOH remains a fixed value. The CNN–GRU–AM deep learning model is used for SOH update during the battery resting stage. The joint estimation schematic diagram is shown in Fig. 7. The SOC is estimated on the local, SOH is calculated on the remote

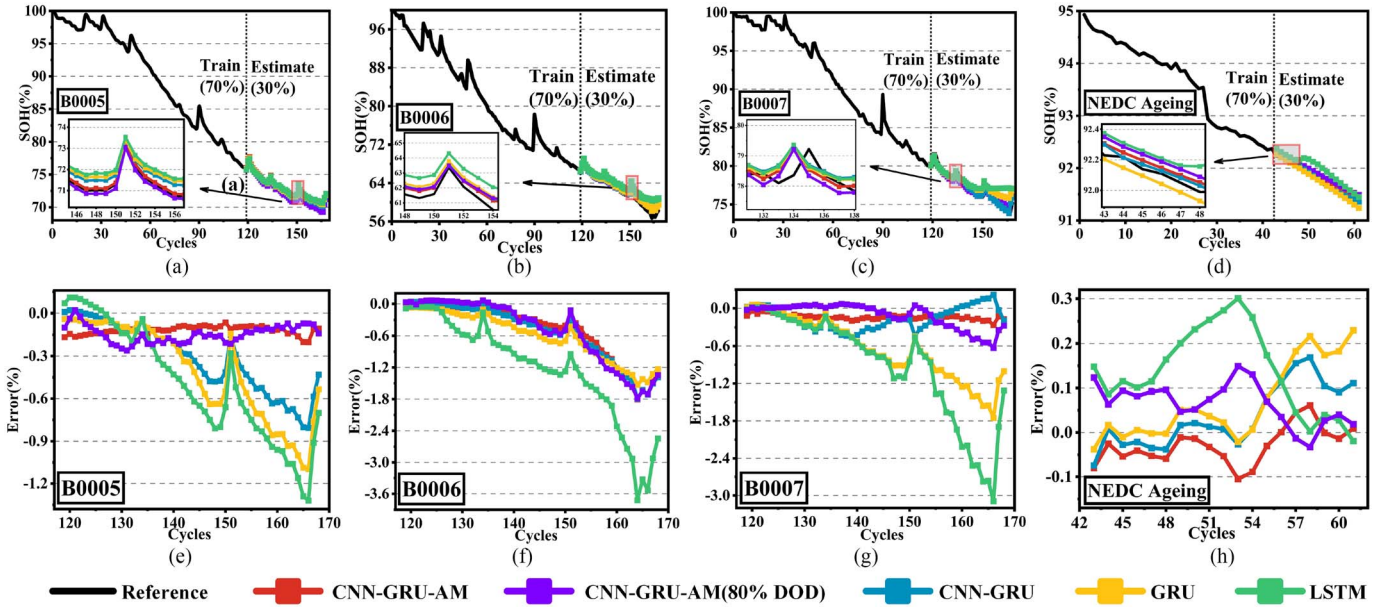

Fig. 6. SOH estimation. (a) SOH estimation with B0005. (b) SOH estimation with B0006. (c) SOH estimation with B0007. (d) SOH estimation under NEDC aging. (e) Error of SOH estimation with B0005. (f) Error of SOH estimation with B0006. (g) Error of SOH estimation with B0007. (h) Error of SOH estimation under NEDC aging.

TABLE IV
MAE AND RMSE OF SOH ESTIMATION UNDER DIFFERENT MODELS AND TEST CONDITIONS

Model	Criteria	B0005	B0006	B0007	NEDC Aging
LSTM	MAE (%)	0.51	1.22	0.90	0.14
	RMSE (%)	0.63	1.56	1.24	0.17
GRU	MAE (%)	0.40	0.60	0.64	0.07
	RMSE (%)	0.52	0.75	0.80	0.11
CNN–GRU	MAE (%)	0.31	0.53	0.19	0.06
	RMSE (%)	0.40	0.75	0.23	0.08
CNN–GRU–AM	MAE (%)	0.12	0.48	0.13	0.04
	RMSE (%)	0.12	0.72	0.14	0.05
CNN–GRU–AM (80% DOD)	MAE (%)	0.15	0.53	0.14	0.07
	RMSE (%)	0.16	0.77	0.22	0.08

computation, so that the computing resources can be allocated reasonably.

B. Experimental Validation

The experiment validation platform is presented as shown in Fig. 8. The battery experimental equipment comprises 18650VTC6 lithium-ion batteries, an incubator, a 12V direct current (dc) power supply, a bidirectional programmable dc power supply IT-M3412 as load, a current sensor, and a host computer.

The real-time controller for SOC estimation is the FastECU_EQ15, which is with 150 MHz main frequency, 4M FLASH, 192k RAM, and three-way CAN communication channel. CAN 1 channel is used for data transmission and variable calibration with the host; CAN 2 channel is connected with the module of data collection; CAN 3 channel is connected with IT-M3412. The proposed temperature-dependent EKF model is developed on MATLAB/Simulink platform and embedded in the FastECU_EQ15 through code generation. The SOH

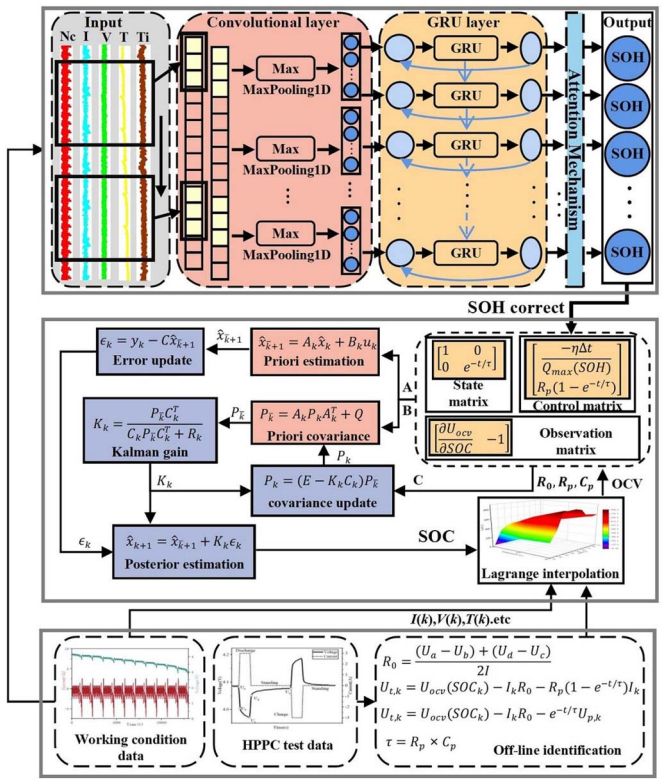

Fig. 7. Schematic diagram of the proposed SOC-SOH joint estimation.

estimation platform is a server provided by AutoDL. Based on Keras deep learning framework and Jupyter Notebook + Tensorflow 2.2.0 backend, SOH is estimated.

At the end of each discharge cycle, the data are collected and calculated by FastECU_EQ15. The data are uploaded to the remote computing platform through the SSH network protocol

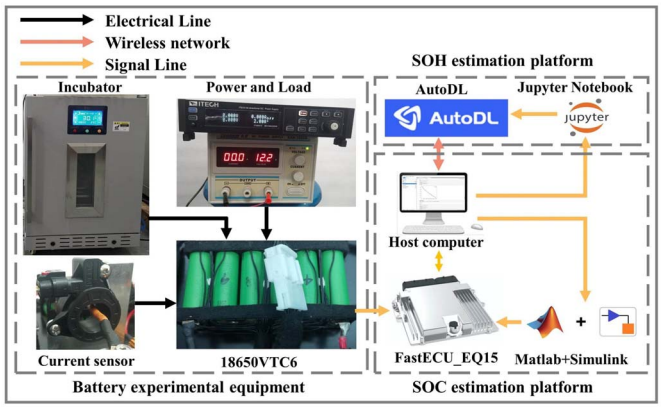

Fig. 8. Joint estimation experimental validation platform.

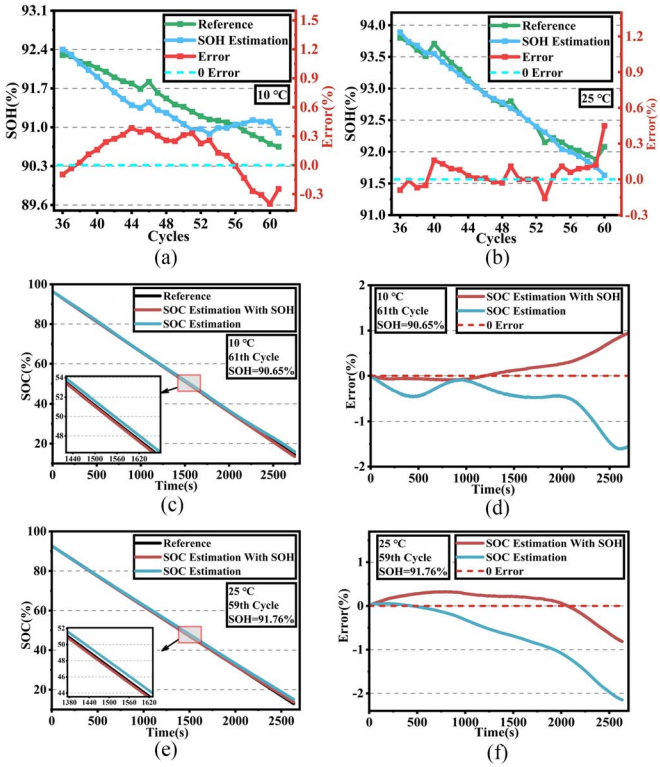

Fig. 9. Joint estimation results under 1C cyclic aging. (a) SOH estimation at 10 °C. (b) SOH estimation at 25 °C. (c) SOC estimation under 90.65% SOH at 10 °C. (d) SOC estimation error at 90.65% SOH at 10 °C. (e) SOC estimation under 91.76% SOH at 25 °C. (f) SOC estimation error at 91.76% SOH at 25 °C.

provided by AutoDL. The model training and SOH estimation are carried out on the remote computing platform, and the SOH estimation results are sent to the FastECU_EQ15 to correct the maximum available capacity.

To verify the feasibility of the proposed dual time-scale estimation of SOC–SOH for lithium-ion battery, cyclic aging experiments were performed on the batteries according to the validation platform in Fig. 8. The lithium-ion batteries were placed in incubators at 10 °C and 25 °C, respectively. The batteries were fully charged through CC–CV, and then discharged at 1C (3A) cycle. At 1C discharge rate, SOH decreased to 90.65% and 91.97% for 61 cycles. The training dataset used for the CNN–GRU–AM-based SOH estimation at the remote computing platform is the data of the first 35 cycle discharge processes at 10 °C and 25 °C. The training sets were 596,870 and 614,705 pieces of data, respectively. The training time of the model was 657 s and 864 s, respectively. The SOH after the 36th discharge was calculated and updated. SOH is a constant during the battery discharge. The SOH estimation results are shown in Fig. 9(a) and 9(b) and Table V. The CNN–GRU–AM model can track the SOH accurately, and the maximum error was no more than 0.6%.

TABLE V
MAE AND RMSE OF JOINT ESTIMATION UNDER 1C CYCLIC AGING

Model	Criteria	10 °C	25 °C
SOH estimation	MAE (%)	0.23	0.08
	RMSE (%)	0.25	0.12
SOC estimation with SOH	MAE (%)	0.23	0.25
	RMSE (%)	0.34	0.29
SOC estimation	MAE (%)	0.73	0.67
	RMSE (%)	1.02	0.89

The sampling time of the local controller FastECU_EQ15 real-time SOC calculation is 0.1s. The SOC estimation results for the 61st cycle at 10 °C and the 59th cycle at 25°C are shown in Fig. 9 (c) and 9(d). The accuracy of SOC estimation with updated SOH was better than the results without SOH updating.

In particular, after the 2000 s, the SOC estimation without SOH updating was greater than the reference value, which may lead to battery over discharge. The MAEs and RMSEs of SOC estimation errors considering SOH updates were less than 0.5%. In the future, after carrying out battery aging experiments under a wider range of temperatures and dynamic conditions, joint SOC–SOH estimation studies can be conducted throughout the battery's entire life cycle.

V. CONCLUSION

In this article, the temperature-dependent EKF developed in real-time controller and CNN–GRU–AM at remote computing platform are designed for SOC–SOH joint estimation. The battery model parameters, R_0, R_p, C_p, and U_{ocv} at experimental temperatures are formulated by Lagrange interpolation, and SOC is estimated in real-time by EKF method. Under the NEDC test condition, RMSEs of the proposed model output voltage were less than 20 mV; the SOC estimations were better than without temperature consideration, and the errors were less than 1%. The CNN–GRU–AM model is trained on a remote computing platform to capture aging features for SOH estimation. To verify the deep learning CNN–GRU–AM battery model, the estimation errors of SOH in the NASA dataset and NEDC aging tests were less than 1%. Finally, according to the SOH estimation achieved by the remote computing platform, the maximum available capacity variable in the control matrix of EKF model is updated to improve the accuracy of SOC estimation next

time. Therefore, the dual time-scale joint estimation of SOC–SOH is realized. The proposed SOC–SOH joint estimation was verified by 1C discharge rate experiment at 10 °C and 25 °C. The accuracy of SOC and SOH estimation remained within 1%. The proposed joint estimation method, combining local real-time controller and remote computing platforms, can reduce the burden of local hardware and memory. In the future research work, the remote computing platform will be further used to realize cloud collaborative joint estimation and process high-precision complex mechanism models.

REFERENCES

[1] W. Yan, B. Zhang, G. Zhao, S. Tang, G. Niu, and X. Wang, "A battery management system with a Lebesgue-sampling-based extended Kalman filter," *IEEE Trans. Ind. Electron.*, vol. 66, no. 4, pp. 3227–3236, Apr. 2019.

[2] Q. Zhang, et al., "State-of-health estimation of batteries in an energy storage system based on the actual operating parameters," *J. Power Sources*, vol. 506, Sept. 2021, Art. no. 230162.

[3] Y. Wang, et al., "A comprehensive review of battery modeling and state estimation approaches for advanced battery management systems," *Renew. Sust. Energ. Rev*, vol. 131, Oct. 2020, Art. no. 110015.

[4] Y. Fu, J. Xu, M. Shi, and X. Mei, "A fast impedance calculation-based battery state-of-health estimation method," *IEEE Trans. Ind. Electron.*, vol. 69, no. 7, pp. 7019–7028, Jul. 2022.

[5] F. Yang, W. Li, C. Li, and Q. Miao, "State-of-charge estimation of lithium-ion batteries based on gated recurrent neural network," *Energy*, vol. 175, pp. 66–75, May 2019, doi: 10.1016/j.energy.2019.03.059.

[6] S. Dey, Y. Shi, K. Smith, A. Colclasure, and X. Li, "From battery cell to electrodes: real-time estimation of charge and health of individual battery electrodes," *IEEE Trans. Ind. Electron.*, vol. 67, no. 3, pp. 2167–2175, Mar. 2020.

[7] Q. Zhang, C.-G. Huang, H. Li, G. Feng, and W. Peng, "Electrochemical impedance spectroscopy based state-of-health estimation for lithium-ion battery considering temperature and state-of-charge effect," *IEEE Trans. Transp. Electrific.*, vol. 8, no. 4, pp. 4633–4645, Dec. 2022.

[8] X. Shu, Z. Chen, J. Shen, F. Guo, Y. Zhang, and Y. Liu, "State of charge estimation for lithium-ion battery based on hybrid compensation modeling and adaptive H-infinity filter," *IEEE Trans. Transp. Electrific.*, vol. 9, no. 1, pp. 945–957, Mar. 2023.

[9] Z. Du, L. Zuo, J. Li, Y. Liu, and H. T. Shen, "Data-driven estimation of remaining useful lifetime and state of charge for lithium-ion battery," *IEEE Trans. Transp. Electrific.*, vol. 8, no. 1, pp. 356–367, Mar. 2022.

[10] H. Wang, G. Zhou, J. Xu, Z. Liu, X. Yan, and J. A. McCann, "A simplified historical-information-based SOC prediction method for supercapacitors," *IEEE Trans. Ind. Electron.*, vol. 69, no. 12, pp. 13090–13098, Dec. 2022.

[11] Y.-X. Wang, Z. Chen, and W. Zhang, "Lithium-ion battery state-of-charge estimation for small target sample sets using the improved GRU-based transfer learning," *Energy*, vol. 244, no. Part B, Apr. 2022. Art. no. 123178.

[12] X. Shu, G. Li, Y. Zhang, S. Shen, Z. Chen, and Y. Liu, "Stage of charge estimation of lithium-ion battery packs based on improved cubature Kalman filter with long short-term memory model," *IEEE Trans. Transp. Electrific.*, vol. 7, no. 3, pp. 1271–1284, Sep. 2021.

[13] F. Naseri, E. Schaltz, D.-I. Stroe, A. Gismero, and E. Farjah, "An enhanced equivalent circuit model with real-time parameter identification for battery state-of-charge estimation," *IEEE Trans. Ind. Electron.*, vol. 69, no. 4, pp. 3743–3751, Apr. 2022.

[14] Y. Gao, K. Liu, C. Zhu, X. Zhang, and D. Zhang, "Co-estimation of state-of-charge and state-of-health for lithium-ion batteries using an enhanced electrochemical model," *IEEE Trans. Ind. Electron.*, vol. 69, no. 3, pp. 2684–2696, Mar. 2022.

[15] X. Shu, G. Li, J. Shen, W. Yan, Z. Chen, and Y. Liu, "An adaptive fusion estimation algorithm for state of charge of lithium-ion batteries considering wide operating temperature and degradation," *J. Power Sources*, vol. 462, Jun. 2020, Art. no. 228132.

[16] X. Tang, Y. Wang, K. Yao, Z. He, and F. Gao, "Model migration based battery power capability evaluation considering uncertainties of temperature and aging," *J. Power Sources*, vol. 440, Nov. 2019, Art. no. 227141.

[17] J. Tian, R. Xiong, and W. Shen, "State-of-health estimation based on differential temperature for lithium ion batteries," *IEEE Trans. Power Electron.*, vol. 35, no. 10, pp. 10363–10373, Oct. 2020.

[18] J. Tian, R. Xiong, and Q. Yu, "Fractional-order model-based incremental capacity analysis for degradation state recognition of lithium-ion batteries," *IEEE Trans. Ind. Electron.*, vol. 66, no. 2, pp. 1576–1584, Feb. 2019.

[19] T. Ouyang, P. Xu, J. Lu, X. Hu, B. Liu, and N. Chen, "Coestimation of state-of-charge and state-of-health for power batteries based on multithread dynamic optimization method," *IEEE Trans. Ind. Electron.*, vol. 69, no. 2, pp. 1157–1166, Feb. 2022.

[20] C. Jiang, S. Wang, B. Wu, C. Fernandez, X. Xiong, and J. Coffie-Ken, "A state-of-charge estimation method of the power lithium-ion battery in complex conditions based on adaptive square root extended Kalman filter," *Energy*, vol. 219, Mar. 2021, Art. no. 119603.

[21] Y. Fan, F. Xiao, C. Li, G. Yang, and X. Tang, "A novel deep learning framework for state of health estimation of lithium-ion battery," *J. Energy Storage*, vol. 32, Dec. 2020, Art. no. 101741.

[22] Y. Zhang, Y. Wang, Y. Xia, and W. Chen, "A deep learning approach to estimate the state of health of lithium-ion batteries under varied and incomplete working conditions," *J. Energy Storage*, vol. 58, Feb. 2023, Art. no. 106323.

[23] W. Zhang, L. Wang, L. Wang, C. Liao, and Y. Zhang, "Joint state-of-charge and state-of-available-power estimation based on the online parameter identification of lithium-ion battery model," *IEEE Trans. Ind. Electron.*, vol. 69, no. 4, pp. 3677–3688, Apr. 2022.

[24] B. Jiang, H. Dai, X. Wei, and T. Xu, "Joint estimation of lithium-ion battery state of charge and capacity within an adaptive variable multi-timescale framework considering current measurement offset," *Appl. Energy*, vol. 253, Nov. 2019, Art. no. 113619.

[25] Y. Li et al., "A hybrid machine learning framework for joint SOC and SOH estimation of lithium-ion batteries assisted with fiber sensor measurements," *Appl. Energy*, vol. 325, Nov. 2022, Art. no. 119787.

[26] Y. Song, D. Liu, H. Liao, and Y. Peng, "A hybrid statistical data-driven method for on-line joint state estimation of lithium-ion batteries," *Appl. Energy*, vol. 261, Mar. 2020, Art. no. 114408.

[27] Z. Wei, G. Dong, X. Zhang, J. Pou, Z. Quan, and H. He, "Noise-immune model identification and state-of-charge estimation for lithium-ion battery using bilinear parameterization," *IEEE Trans. Ind. Electron.*, vol. 68, no. 1, pp. 312–323, Jan. 2021.

[28] M. Kwak, B. Lkhagvasuren, J. Park, and J.-H. You, "Parameter identification and SOC estimation of a battery under the hysteresis effect," *IEEE Trans. Ind. Electron.*, vol. 67, no. 11, pp. 9758–9767, Nov. 2020.

[29] G. Dong, W. Han, and Y. Wang, "Dynamic Bayesian network-based lithium-ion battery health prognosis for electric vehicles," *IEEE Trans. Ind. Electron.*, vol. 68, no. 11, pp. 10949–10958, Nov. 2021.

[30] L. Wang, D. Lu, Q. Liu, L. Liu, and X. Zhao, "State of charge estimation for LiFePO4 battery via dual extended Kalman filter and charging voltage curve," *Electrochim. Acta*, vol. 296, pp. 1009–1017, Feb. 2019, doi: 10.1016/j.electacta.2018.11.156.

[31] L. Li, Y. Li, R. Mao, L. Li, W. Hua, and J. Zhang, "Remaining useful life prediction for lithium-ion batteries with a hybrid model based on TCN-GRU-DNN and dual attention mechanism," *IEEE Trans. Transp. Electrific.*, vol. 9, no. 3, pp. 4726–4740, Sept. 2023.

[32] Q. Yao, D. D.-C. Lu, and G. Lei, "A surface temperature estimation method for lithium-ion battery using enhanced GRU-RNN," *IEEE Trans. Transp. Electrific.*, vol. 9, no. 1, pp. 1103–1112, Mar. 2023.

[33] B. Saha and K. Goebel, "Battery Data Set," NASA Prognostics Data Repository, NASA Ames Research Center, Moffett Field, CA, USA, 2007. [Online]. Available: https://www.nasa.gov/intelligent-systems-division/discovery-and-systems-health/pcoe/pcoe-data-set-repository/

Shiquan Wang received the B.Eng. degree in vehicle engineering from Fujian Agriculture and Forestry University, Fuzhou, China, in 2022. He is currently working toward the M.Eng. degree in mechanical engineering with Fuzhou University, Fuzhou.

His research interests include lithium-ion battery modeling and state estimation.

Kai Ou received the B.Eng. degree from Wenzhou University, Wenzhou, China, in 2014, and the Ph.D. degree from Chonnam National University, Gwangju, Republic of Korea, in 2019, both in mechanical engineering.

From 2019 to 2020, he worked as a Postdoctoral Research Associate with Chonnam National University. He is currently an Associate Professor with the School of Mechanical Engineering and Automation, Fuzhou University, Fuzhou, China. His research interests include proton exchange membrane fuel cell modeling and control, and hybrid power systems energy management.

Wei Zhang received the B.S. degree in informatik from the Universität Stuttgart, Stuttgart, Germany, in 2008, and the M.S. degree in automotive software engineering from the Technische Universität Chemnitz, Chemnitz, Germany, in 2012. He is currently working toward the Ph.D. degree with the Institute for Electrical Drive Systems and Power Electronics, Technische Universität München, Munich, Germany.

He is currently the CEO of Geo Micro Devices (Xiamen) Co. Ltd., Xiamen, China. His research interests include learning-based control theory for electrical drives, robotics, mechanical system, laser system, and deep learning in industrial computer vision.

Ya-Xiong Wang (Member, IEEE) received the M.Eng. and Ph.D. degrees in mechanical engineering from Chonnam National University, Gwangju, Republic of Korea, in 2012 and 2015, respectively.

He is currently a Professor with the School of Mechanical Engineering and Automation, Fuzhou University, Fuzhou, China. His research interests include proton exchange membrane fuel cell modeling and control, battery management system, hybrid renewable power systems energy management, and artificial intelligence for energy.